Atendra Kumar[1]
Department of Mathematics,
National Institute of Technology Srinagar,
Hazratbal, Srinagar 190006, India;
Department of Computational and Data Sciences,
Indian Institute of Science Bangalore,
Bangalore 560012, India
e-mail: atendra@nitsri.net

Rajendra K. Ray
School of Basic Sciences,
Indian Institute of Technology Mandi,
Kamand, Mandi 175005, India

H. V. R. Mittal
Computer, Electrical and Mathematical Sciences
and Engineering Division,
King Abdullah University of Science and
Technology,
Thuwal 23955-6900, Saudi Arabia;
Department of Mathematics,
Indian Institute of Technology Palakkad,
Ahalia Integrated Campus,
Kozhippara, Palakkad 678557, India

Heat Transfer Past a Rotationally Oscillating Circular Cylinder in Linear Shear Flow

This study investigates the unsteady, two-dimensional flow and heat transfer past a rotationally oscillating circular cylinder in linear shear flow. A higher order compact (HOC) finite difference scheme is used to solve the governing Navier–Stokes equations coupled with the energy equation on a nonuniform grid in polar coordinates. The hydrodynamic and thermal features of the flow are mainly influenced by the shear rate (K), Reynolds number (Re), Prandtl number (Pr), and the cylinder oscillation parameters, i.e., oscillation amplitude (α_m), the frequency ratio (f_r). The simulations are performed for $Re = 100, Pr = 0.5 - 1.0$, $0.0 \leq K \leq 0.15$, and $0.5 \leq \alpha_m \leq 2.0$. The numerical scheme is validated with the existing literature studies. Partial and full vortex suppression is observed for certain values of shear parameter K. The connection between heat transfer and vortex shedding phenomenon is examined where a pronounced increase in the heat transfer is observed for certain values of oscillation parameter, relative to the nonshear flow case. [DOI: 10.1115/1.4054350]

Keywords: circular cylinder, rotational oscillation, heat transfer, shear flow, finite difference, Navier–Stokes equations

1 Introduction

Fluid flow and heat transfer around bluff bodies like circular cylinders have been a subject of great importance. Consequently, this subject is well-studied due to its practical applications and theoretical considerations [1–7]. Major applications encompass several industrial processes like tube-tank heat exchangers [8], eolian tones [9], flow control [10,11], mooring lines [12], offshore oil platforms [13,14], etc. Further applications are in the chips of various shapes and cooling of electronic components [15,16].

Most of the literature studies consider nonshear flows around circular cylinders for their experiments [13,17–24] and references therein. However, in reality, the nature of these flows is not exactly nonshear. Thus, they can be better demonstrated by considering their shear nature. An efficient way of simulating such flows is by considering a linear velocity profile with a constant shear at the inlet. For instance, a typical structure in the atmospheric boundary layer where a velocity gradient exists in the freestream. In fact, when the inflow freestream is a shear flow, it causes a troublesome interaction of the free shear layer with the boundary layer of the cylinder. This is due to the background vorticity in the freestream which further alters the wake structure, vortex shedding pattern, and the aerodynamic forces in a significant way. It is known that in the case of shear flows, vortex shedding is suppressed beyond a critical shear parameter value. This causes a significant reduction in the drag force [25]. Such flows also furnish details of new observations which help to understand the heat transfer mechanism in the case of heated cylinders. It is well established that there is a strong coupling between the vortex shedding and heat transfer. A significant enhancement of heat transfer has been observed under certain forcing conditions, in the case of oscillating cylinders in nonshear flows. Saxena and Laird [26] reported that the forced oscillation of the cylinder results in a significant enhancement of heat transfer as the oscillation frequency of the cylinder approaches the vortex shedding frequency. Leung et al. [27] reported heat transfer enhancement with increasing either amplitude of oscillation or frequency at higher Reynolds numbers 3000 to 50000. Childs and Mayle [28] carried out a theoretical investigation on the effect of rotational oscillations on heat transfer for very small amplitudes of oscillations. The results showed no enhancements in heat transfer which was attributed to the boundary layer assumptions. Chin Hsiang et al. [29] reported that the coefficient of heat transfer can be significantly increased by the oscillation of the cylinder for $0 \leq Re \leq 4000$. Moreover, they noted that the lock-on and turbulence effects also play important roles in the heat transfer mechanism. Mahfouz and Badr [19] studied the forced convection from a heated cylinder with rotational oscillation placed in a nonshear stream. Their results show the occurrence of the lock-on phenomenon within a band of frequencies close to the natural frequency. Further, a significant enhancement in the heat transfer is observed within the lock-on frequency range. Fu and Tong [30] numerically studied the flow structures and heat transfer characteristics of a heated cylinder oscillating transversely. They concluded that the interaction of oscillating cylinder and vortex shedding dominates the wake leading to the periodicity of thermal fields in the lock-on regime. As a result, the heat transfer is enhanced remarkably. Ghazanfarian and Nobari [23,24] analyzed the mechanism of heat transfer from a rotating circular cylinder performing cross and inline oscillations. The results showed that the heat transfer is increased significantly in the lock-on regime and vortex shedding is suppressed beyond a critical rotation speed. Also, the average Nusselt number and the drag coefficient decrease rapidly with an increase in the rotational speed of the cylinder. Heat transfer improvement in a channel over a rotationally oscillating cylinder was analyzed by Beskok et al. [31]. They reported that the maximum heat transfer was acquired when the oscillating frequency is 80% of the vortex shedding frequency of the fixed cylinder. Meanwhile, the analysis of the heat transfer phenomenon from a fixed heated cylinder with the circular motion in a nonshear stream was done by AlMdallal and Mahfouz [32]. He observes a significant increase in heat transfer rate with increasing amplitude of circular motion.

However, very few studies exist in the literature for flows past circular cylinders subject to shear flows. For instance, fixed circular cylinders by Jordan and Fromm [33], Cao et al. [34–36], Wu and Chen [37], Lei et al. [38], Sumner and Akosile [39], Kappler

[1]Corresponding author.
Contributed by the Heat Transfer Division of ASME for publication in the Journal of Heat Transfer. Manuscript received September 27, 2021; final manuscript received April 8, 2022; published online May 11, 2022. Assoc. Editor: Ranga Narayanan.

et al. [40], Singh and Mittal [25], Kim et al. [41], Kang [42], Omori et al. [43], Zhang et al. [44], Kumar and Ray [7]; rotating circular cylinders by Yoshino and Hayashi [45], Kurose and Komori [46], Kang [47], Rohlf and D'Alessio [48], Chew et al. [49] and oscillating cylinders by Stansby [50]. Most of these studies primarily focused on the phenomenon of vortex shedding suppression, lift force, drag crisis, movement of stagnation, etc. Partial and full vortex shedding suppression is determined for a range of parameter values together with the nature of hydrodynamic forces acting on the cylinder. It is worth mentioning that none of the studies discussed above considered heat convection phenomena. Only a handful of studies existing in the literature investigate heat transfer phenomena past circular cylinders subject to shear flow. Shi et al. [51] studied the heat transfer characteristics of shear flow past fixed cylinders placed near a wall. Their results show a significant effect of shear rate on local Nusselt number and almost no effect on the value of average Nusselt number. Abdella and Nalitolela [52] studied heat transfer past a rotating circular cylinder in shear flow. They observed significant variation in local Nusselt number distribution with the shear rate for a fixed rotation speed of the cylinder. The problem of heat transfer past a rotating circular cylinder in shear flow is also investigated by Nemati et al. [53]. Their results show that the local Nusselt number at the surface of the cylinder tends to shift in the direction of rotation. But the maximum value remains fixed at the front stagnation point ($\theta = \pi$). To the best of our knowledge, no study has considered heat transfer past a rotationally oscillating circular cylinder subject to shear flow, which is investigated in the present work. The effect of incoming shear on the heat transfer mechanism around the cylinder is investigated by analyzing local Nusselt number plots, average Nusselt number plots, and isotherm contours for a wide range of numerical parameters. The modes of vortex shedding in the lock-on regions are presented and classified for $Re = 100$, $f_r = 1.0$, $Pr = 0.5-1.0$, $\alpha_m \in [0.5, 2.0]$, $K \in [0.0, 0.15]$. A thorough study of the relationship between the above-mentioned parameters and heat transfer is done to investigate the effect of shear flow ($K = 0.05, 0.1, 0.15$) relative to the nonshear flow cases ($K = 0.0$). We have described the vortex shedding modes as per the number of vortices shed from each side of the cylinder in a lock-on period, $T_p = mT$ (where m is a real number) following the works of Ongoren and Rockwell [54], Williamson et al. [55], Al-Mdallal et al. [56], Mittal et al. [4]. Here, T is the period of the cylinder oscillation and T_p is the lock-on period. For example, the nS mode per T, i.e., $nS(T)$, refers to the shedding of n vortices from either side of the cylinder or alternate shedding counter-rotating $n/2$ vortices from each side of the cylinder over one cylinder oscillating period, T.

The paper is organized in the following sequence. In Sec. 2, we describe the governing equations and their discretization procedure in the Sec. 3. Section 4 deals with validation of the numerical scheme followed by results and discussion in Sec. 5. Finally, we summarize our observations in the conclusion.

2 Governing Equations

The problem of unsteady, incompressible, viscous, shear flow of constant property Newtonian fluid past an infinitely long circular cylinder of radius $R_\circ$ is considered in the present study. Figure 1 sketches the two-dimensional schematic diagram of the problem domain together with a photograph of the computational grid. The fluid flow advances toward the cylinder with a linear shear velocity $u = U_o + Ky, v = 0$, which is in polar coordinates can be written as

$$u = (U_o + Kr\sin\theta)\cos\theta, v = -(U_o + Kr\sin\theta)\sin\theta \tag{1}$$

and uniform temperature T_∞, where U_o is the space-averaged centerline velocity of inflow and K is the shear parameter. Notice that the cylinder performs rotational oscillations around its axis with velocity, $\alpha(t)$, such that

$$\alpha(t) = \alpha_m \sin(2\pi f t) \tag{2}$$

The conservation equations that govern the two-dimensional flow motion are the continuity and momentum equations. The analysis of heat transfer is based on the two-dimensional unsteady thermal energy conservation principle. The dimensionless form of these governing equations in cylindrical polar coordinates (r, θ) can be written as (Ref. [20])

$$\frac{\partial^2\omega}{\partial r^2} + \frac{1}{r}\frac{\partial\omega}{\partial r} + \frac{1}{r^2}\frac{\partial^2\omega}{\partial\theta^2} = \frac{Re}{2}\left\{u\frac{\partial\omega}{\partial r} + \frac{v}{r}\frac{\partial\omega}{\partial\theta} + \frac{\partial\omega}{\partial t}\right\} \tag{3}$$

$$\frac{\partial^2\psi}{\partial r^2} + \frac{1}{r}\frac{\partial\psi}{\partial r} + \frac{1}{r^2}\frac{\partial^2\psi}{\partial\theta^2} = -\omega \tag{4}$$

$$\frac{\partial^2\Theta}{\partial r^2} + \frac{1}{r}\frac{\partial\Theta}{\partial r} + \frac{1}{r^2}\frac{\partial^2\Theta}{\partial\theta^2} = \frac{RePr}{2}\left\{u\frac{\partial\Theta}{\partial r} + \frac{v}{r}\frac{\partial\Theta}{\partial\theta} + \frac{\partial\Theta}{\partial t}\right\} \tag{5}$$

Here ω represents vorticity and ψ for stream function, u and v represents the radial and transverse components of velocity , respectively. The velocity components u, v in terms of stream function ψ can be written as

$$u = \frac{1}{r}\frac{\partial\psi}{\partial\theta}, \quad v = -\frac{\partial\psi}{\partial r} \tag{6}$$

and vorticity ω is

$$\omega = \frac{1}{r}\left[\frac{\partial}{\partial r}(vr) - \frac{\partial u}{\partial\theta}\right] \tag{7}$$

Now, the boundary conditions correlated with Eqs. ((3)–(5)) are explained. On the surface of the cylinder, the boundary conditions for velocity components are those of no-slip, impermeability and isothermal conditions, i.e.

$$u = 0, \qquad v = 0, \qquad \psi = 0, \frac{\partial\psi}{\partial r} = -\alpha \quad \text{and } \Theta = 1 \text{ when } \quad r = 1 \tag{8}$$

The surface vorticity condition can be approximated by using Eq. (4) together with the condition (8) is given as

$$\omega = \frac{\alpha}{r} - \frac{\partial^2\psi}{\partial r^2} \qquad \text{when} \qquad r = 1 \tag{9}$$

The far-field circular boundary is divided into inlet and outlet boundaries, i.e., $x \le 0$ and $x > 0$, respectively. The origin is at the center of the cylinder. At the inlet, a linear shear flow condition

$$u = (U_o + Kr\sin\theta)\cos\theta, v = -(U_o + Kr\sin\theta)\sin\theta \tag{10}$$

is applied whereas the convective boundary condition

$$\frac{\partial\phi}{\partial t} + U_o\frac{\partial\phi}{\partial r} = 0 \tag{11}$$

for all variables , i.e., $\phi = u, v, \psi$, or ω in the radial direction is applied at outlet. The inlet boundary condition for stream function is approximated by using Eq. (6) given below

$$\psi = \left(r - \frac{1}{r}\right)\sin\theta + \frac{K}{4}\left(\frac{1}{r} - 1\right) - \frac{K}{2}\left(r^2 - \frac{1}{r^2}\right)\sin^2\theta \tag{12}$$

while the vorticity at the inlet is obtained by the kinematic definition of vorticity given in Eq. (4) as (Milne-Thomson [57])

$$\omega = -K \tag{13}$$

and

$$\Theta = 0 \tag{14}$$

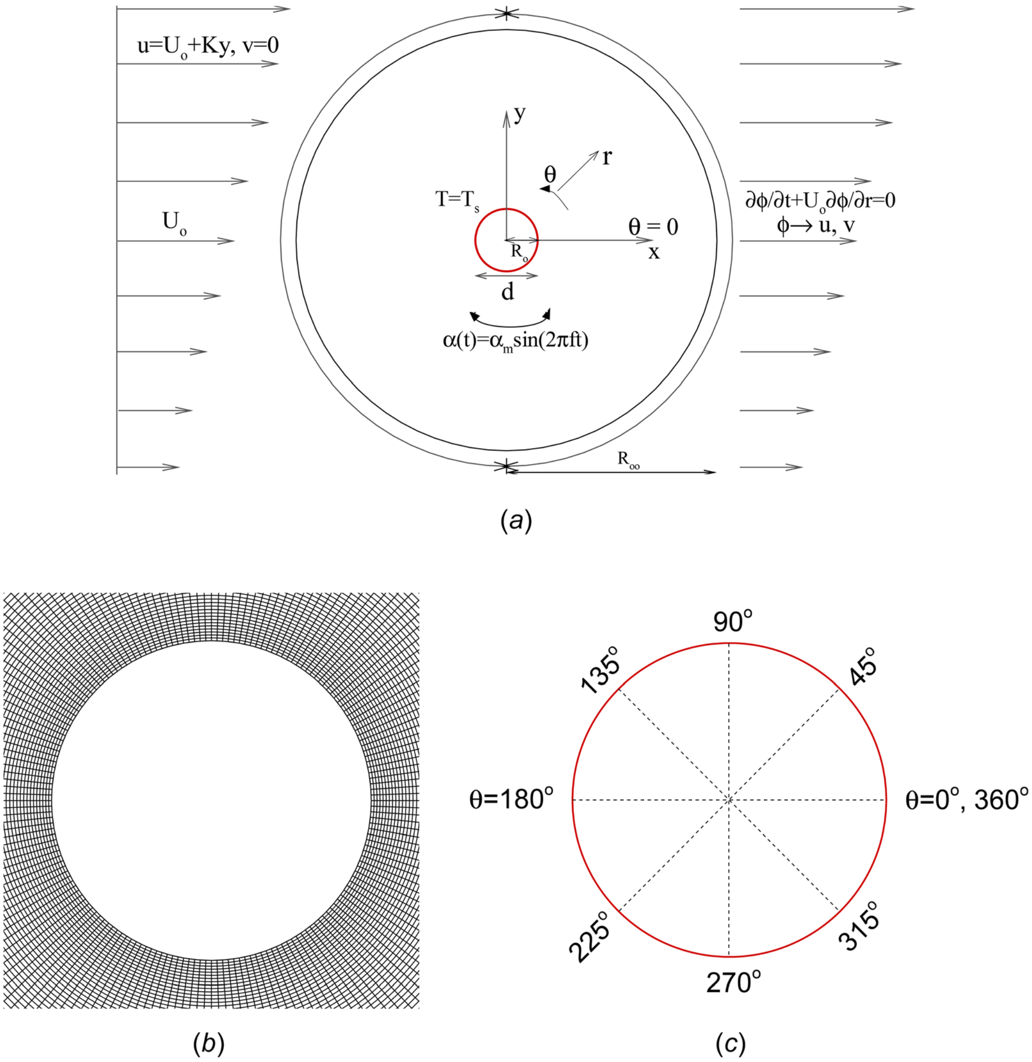

Fig. 1 **(*a*) Schematic diagram of the flow domain, here $\phi = u, v, \psi$, or ω, (*b*) non-uniform polar mesh around the cylinder, and (*c*) close up view of the cylinder**

Since the fully developed flow is independent of initial conditions, all the simulations may be started with arbitrary initial conditions. Also, the periodic characteristic of the solution requires that

$$\omega|_{\theta=0} = \omega|_{\theta=2\pi}, \quad \psi|_{\theta=0} = \psi|_{\theta=2\pi}, \quad \Theta|_{\theta=0} = \Theta|_{\theta=2\pi} \tag{15}$$

2.1 Heat Transfer Parameters. Initially, constant temperature cylinder surface conducts heat to the adjacent layer of fluid followed by its convection with the fluid motion in the wake. The heat conduction from the surface occurs only in the radial direction which affects the radial temperature gradient at the surface followed by its effect on the local radial heat flux. The

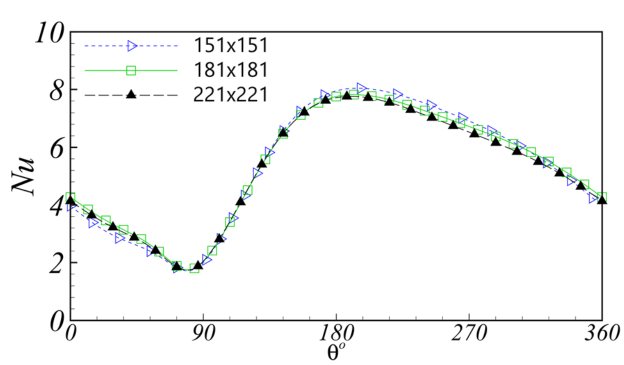

Fig. 2 **Variation of local Nusselt number distribution, *Nu*, over surface of the cylinder computed by present scheme for three different grid sizes 151 × 151, 181 × 181 and 221 × 221 for *Re* = 100, α_m = 0.5, and *K* = 0.1**

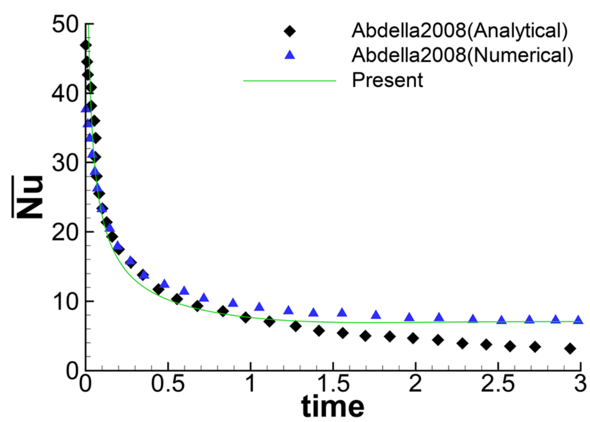

Fig. 3 **Distribution of surface averaged Nusselt number with time at *Re* = 100, α = 0.25, and *K* = 0.1**

Table 1 The values of $\overline{\overline{Nu}}$ for Re=100, α_m=0.5 and K=0.1 by using three different time steps, Δt

Δt	$\overline{\overline{Nu}}$
0.0025	4.0318
0.0050	4.0176
0.0100	4.0019

dimensionless local heat flux in the radial direction is estimated in terms of the local Nusselt number, Nu, defined as

$$Nu = \frac{2hR_0}{k} = \frac{\gamma(2R_0)}{k(T_s - T_\infty)} \quad (16)$$

where h is the local heat transfer coefficient, k represents the thermal conductivity of the fluid and γ represents the surface local radial heat flux defined as $\gamma = -k\frac{\partial T}{\partial r}\big|_{r=R_0}$

Average Nusselt number, $\overline{Nu}$, represents the dimensionless heat transfer from the surface of the cylinder, defined as

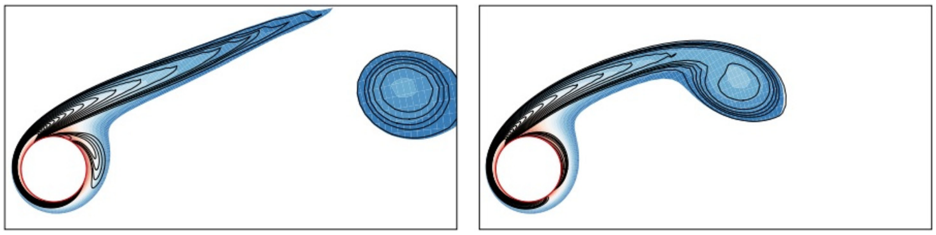

Fig. 4 Isotherm contours superimposed with vorticity contours at times (left) t = 380 and (right) t = 395 for Re = 100, α_m = 0.5, K = 0.1, and f_r = 1.0. Colored contours represent isotherm contours while black lines represent vorticity contours.

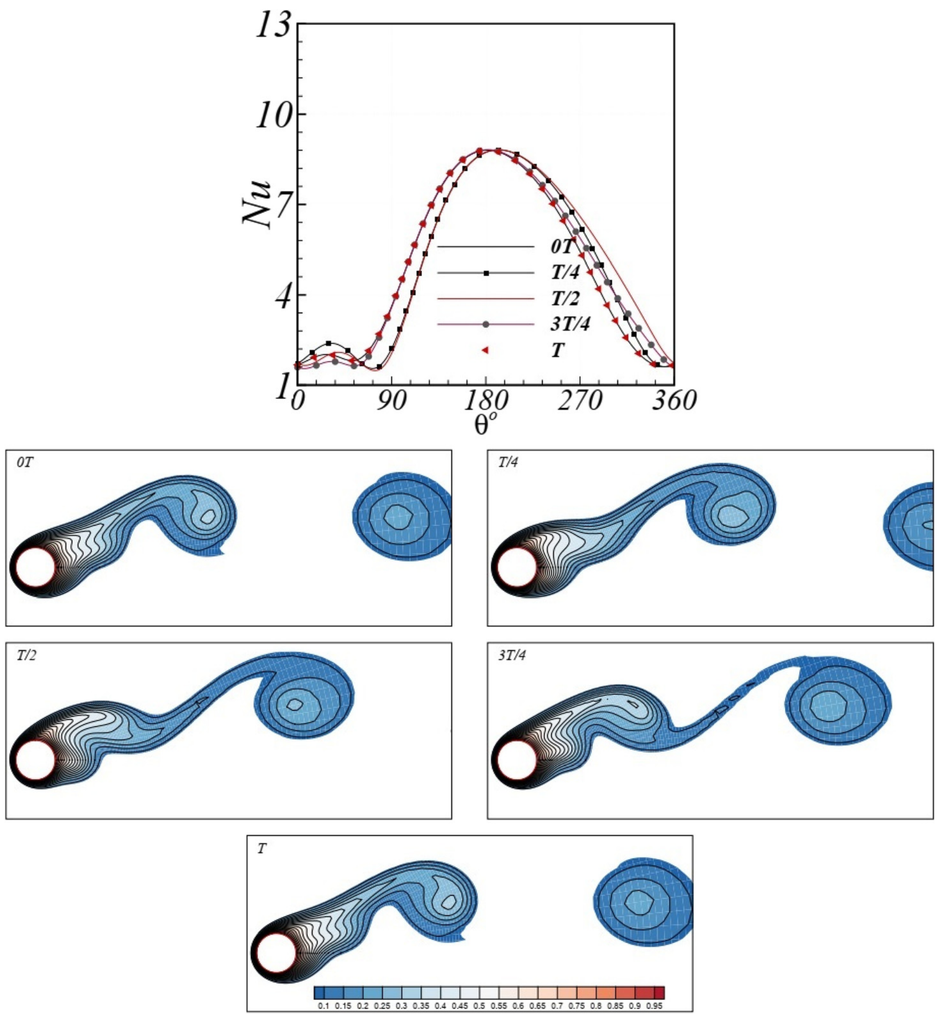

Fig. 5 The variation of local Nusselt number, Nu, along surface of the cylinder and the isotherm contours over one period of cylinder oscillation, T, for Re = 100, α_m = 0.5, and f_r = 1.0, at K = 0.05

$$\overline{Nu} = \frac{2\bar{h}R_0}{k} = \frac{1}{2\pi}\int_0^{2\pi} Nu\, d\theta \tag{17}$$

Here, $\bar{h}$ is the average heat transfer coefficient defined as $\bar{h} = \frac{1}{2\pi}\int_0^{2\pi} h d\theta$. The time-averaged Nusselt number is obtained from

$$\overline{\overline{Nu}} = \frac{1}{t_2 - t_1}\int_{t_1}^{t_2} \overline{Nu} dt \tag{18}$$

where the time period between $t_1 = 200$ and $t_2 = 400$ is taken after the flow reaches the periodic state and covers more than one cycle.

3 Numerical Scheme

The numerical scheme relies on the higher order compact (HOC) finite difference discretization of the governing equations of motion and energy on nonuniform polar grids, similar to the one employed in the work of [7,20]. To discretize the governing Eqs. ((3)–(5)), uniform grid spacing is used along the $\theta-$direction and nonuniform grid spacing in the $r-$direction. To get nonuniform grid spacing along the $r-$direction, we have used the following stretching functions

$$\theta_j = \frac{2\pi}{j_{\max}} \text{ and } r_i = \exp\left(\frac{\lambda\pi i}{i_{\max}}\right)$$

and the grid resolution adjusts by varying the value of the stretching parameter (λ). The HOC discretization of Eqs. ((3)–(4)) is the same as given in Kumar and Ray [7] and is not repeated here for the sake of conciseness. So, it is sufficient to discuss the numerical discretization of the energy Eq. (5). At any grid point (r_i, θ_j), the HOC discretization of Eq. (5) can be given as

$$\begin{aligned}
&[C11_{ij}\delta_r^2 + C12_{ij}\delta_\theta^2 + C13_{ij}\delta_r + C14_{ij}\delta_\theta + C15_{ij}\delta_r\delta_\theta \\
&\quad + C16_{ij}\delta_r\delta_\theta^2 + C17_{ij}\delta_r^2\delta_\theta + C18_{ij}\delta_r^2\delta_\theta^2]\Theta_{ij}^{n+1} \\
&= [C21_{ij}\delta_r^2 + C22_{ij}\delta_\theta^2 + C23_{ij}\delta_r + C24_{ij}\delta_\theta + C25_{ij}\delta_r\delta_\theta \\
&\quad + C26_{ij}\delta_r\delta_\theta^2 + C27_{ij}\delta_r^2\delta_\theta + C28_{ij}\delta_r^2\delta_\theta^2]\Theta_{ij}^{n}
\end{aligned} \tag{19}$$

The detailed expression of the coefficients $C11_{ij}, C12_{ij}, \ldots, C18_{ij}$ and $C21_{ij}, C22_{ij}, \ldots, C28_{ij}$ are presented in the Appendix 1. The detailed expressions of $r_f, r_b, \theta_f, \theta_b$ and the nonuniform difference operators $\delta_r, \delta_r^2, \delta_\theta, \delta_\theta^2$ are given in Appendix 2. The discretization and numerical implementation of the boundary conditions for ψ, u, v, ω and Θ are discussed in [5,7,20]. The heat transfer characteristics and flow physics is determined from the distributions of evolution of dimensionless stream function, vorticity and isotherm contours.

4 Validation

The accuracy and reliability of the scheme on the present model have already been ascertained in the previous works of authors

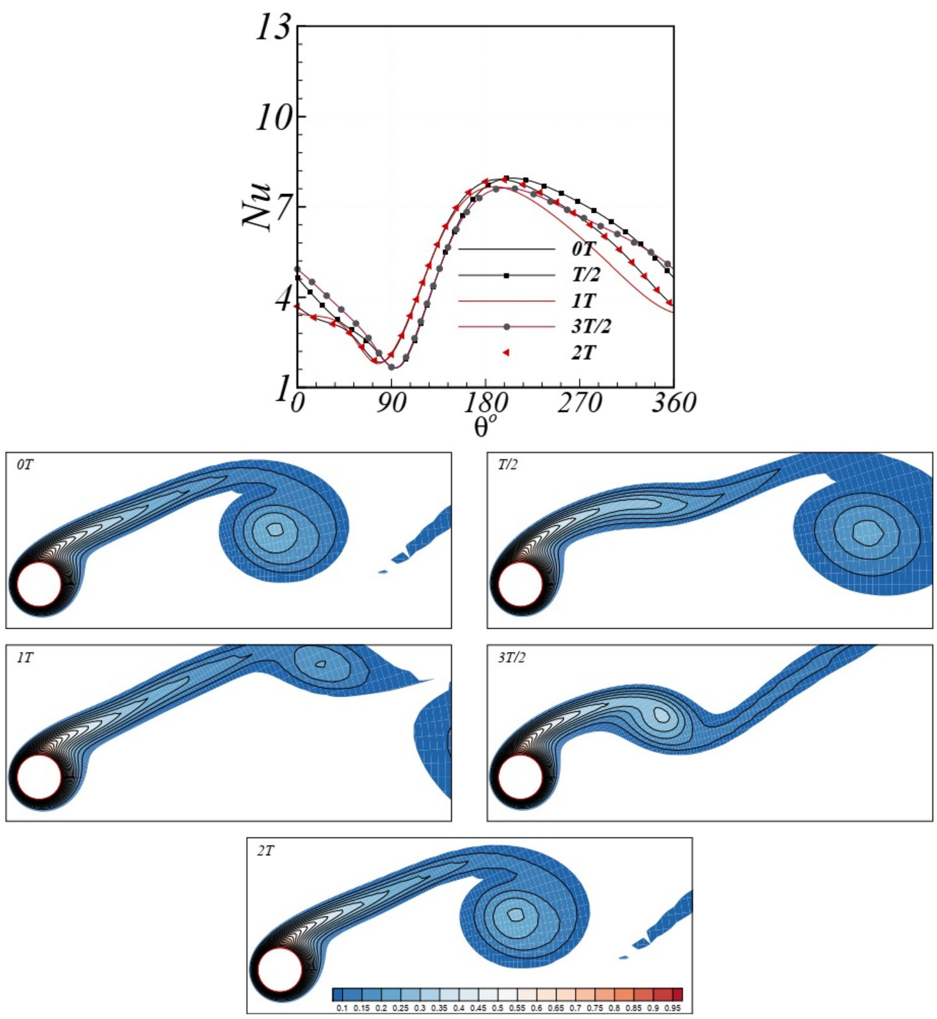

Fig. 6 The variation of local Nusselt number, *Nu*, along surface of the cylinder and the isotherm contours over two periods of cylinder oscillation, 2 *T*, for *Re* = 100, α_m = 0.5, and f_r = 1.0, at *K* = 0.1

[4–7,20]. Investigation is done to determine the optimal choice of grid size, time-step size, and far-field boundary by doing the computation of Nusselt number on three different grid sizes 151×151, 181×181, and 221×221 as shown in Fig. 2. No significant variation in the *Nu* distribution curves is noticed by varying the grid size. Further the time average value of Nusselt number ($\overline{\overline{Nu}}$) is shown for three different time steps Δt as $0.0025, 0.005, 0.01$ (see Table 1). It is found that the maximum relative deviation in $\overline{\overline{Nu}}$ is about 0.9% by varying the time-step from 0.0025 to 0.01. Following the same far-field distance [7], we found that the optimal choice of parameters as grid size 181×181, time-step $\Delta t = 0.01$ and far-field $R_\infty = 25R_\circ$ are sufficient to capture the flow phenomenon accurately.

Further, comparisons have been made with analytical and numerical data available in the literature. Figure 3 shows the comparison between the present result of steadily rotating circular cylinder in shear flow and the corresponding results of Abdella and Nalitolela [52] for the time variation of average Nusselt number, $\overline{Nu}$ at $Re = 100, \alpha = 0.5$ and $K = 0.1$. The present results agree well with the numerical and analytical results.

5 Results and Discussion

The results are presented for different parameter values such as Prandtl number, $Pr = 0.7$; shear rate, $K = 0.0 - 0.15$; oscillation amplitude, $\alpha_m = 0.5 - 2.0$ and frequency ratio $f_r = 1.0$ for a fixed value of Reynolds number, $Re = 100$. Figure 4 exhibits the isotherm contours superimposed with vorticity contours at two different time steps for $\alpha_m = 0.5$, $K = 0.1$, $f_r = 1.0$, and $Re = 100$. It can be seen that the contour of isotherms almost overlaps with the vorticity contours. This indicates that the thermal energy and vorticity generation mechanism experience similar convection and diffusion phenomenon in the flow. The heat is advected from the cylinder wall in the near wake, which is similar to the way vorticity is advected from the cylinder wall. The frequency of vortex shedding and the size of vortices significantly affects the heat convection process because every vortex carries a certain amount of heat [19,20].

Figure 5 displays the isotherm contours and local Nusselt number distribution plots along surface of the cylinder over one period of cylinder oscillation for $K = 0.05$, $\alpha_m = 0.5$, and $Re = 100$. Here the vortex shedding modes are locked-on over one period of cylinder oscillation and the vortex shedding mode is identified as $1S(T)$. Initial investigation of these isotherm contours show developing vortices like chunks of heated fluid being convected downstream, asymmetrically about $x-$axis. The phenomenon of heat transfer is clear from high concentrations of isotherms close to the cylinder surface and low concentrations away from it. This indicates a very thin thermal boundary layer and hence large temperature gradients near the cylinder surface. Interestingly, the vortices are shed only from the upper surface of the cylinder with one

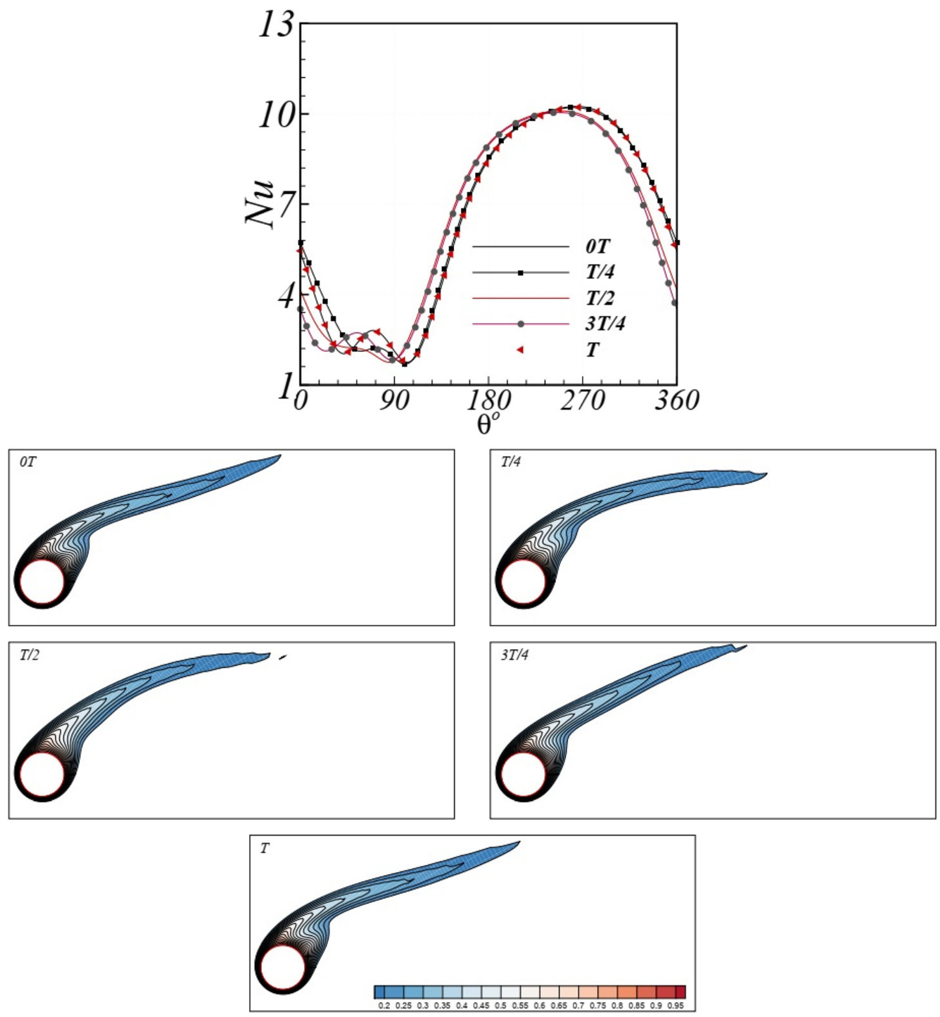

Fig. 7 The variation of local Nusselt number, *Nu*, along surface of the cylinder and the isotherm contours over one period of cylinder oscillation, *T*, for $Re = 100$, $\alpha_m = 0.5$, and $f_r = 1.0$, at $K = 0.15$

vortex shed per one period of cylinder oscillation which is significantly different from the nonshear case (Ref. [20]). The size of the vortices shed is bigger than the nonshear case. This phenomenon is due to the combined effect of the shear rate and oscillations of the cylinder. Further, the wake flow is deflected upwards because of the addition of vorticity generated by rotational oscillations of a cylinder and background negative vorticity due to inlet shear ($\omega = -K$). Figure 5 shows that local Nusselt number distribution at the cylinder surface have the maximum values near the front stagnation point ($\theta \approx 180\,\mathrm{deg}$). The locations of maximum values in Nusselt number distribution also change during cylinder oscillation period in the range $175\,\mathrm{deg} < \theta < 198\,\mathrm{deg}$. This is due to the combined effect of the oscillation amplitude and shear rate. However, the location of maximum peaks in Nusselt number distribution does not show a substantial change in the case of nonshear flow (Ref. [20]). The Nusselt number distribution becomes asymmetric around the front stagnation point because of the asymmetric wall shear gradient. This reveals that the heat transfer mechanism at the upper surface of the cylinder is different from the heat transfer mechanism at the lower surface of the cylinder. Indeed, similar observations were quoted by Nemati et al. [53] for the case of shear flow past a rotating cylinder. An additional local maximum peak in the local Nusselt number distribution curve in the range $20\,\mathrm{deg} < \theta < 50\,\mathrm{deg}$ is observed in Fig. 5. This means the vortex shedding phenomenon causes some enhancement in the heat transfer process in the vicinity of the rear stagnation point similar to the nonshear case.

When the shear rate, K, increases to 0.1, as shown in Fig. 6, the vortex shedding is locked-on over two periods of cylinder oscillation. Here, the vortex shedding mode is identified as $2S(2T)$. The size of the vortices shed is bigger than the size at $K = 0.05$. The value of the maximum peak in the Nusselt number distribution decreases as compared to the case when $K = 0.05$. There is no vortex shedding at the front stagnation point. A lower peak value of the Nusselt number at the front stagnation indicates that more and more heat is being transferred through conduction. The location of

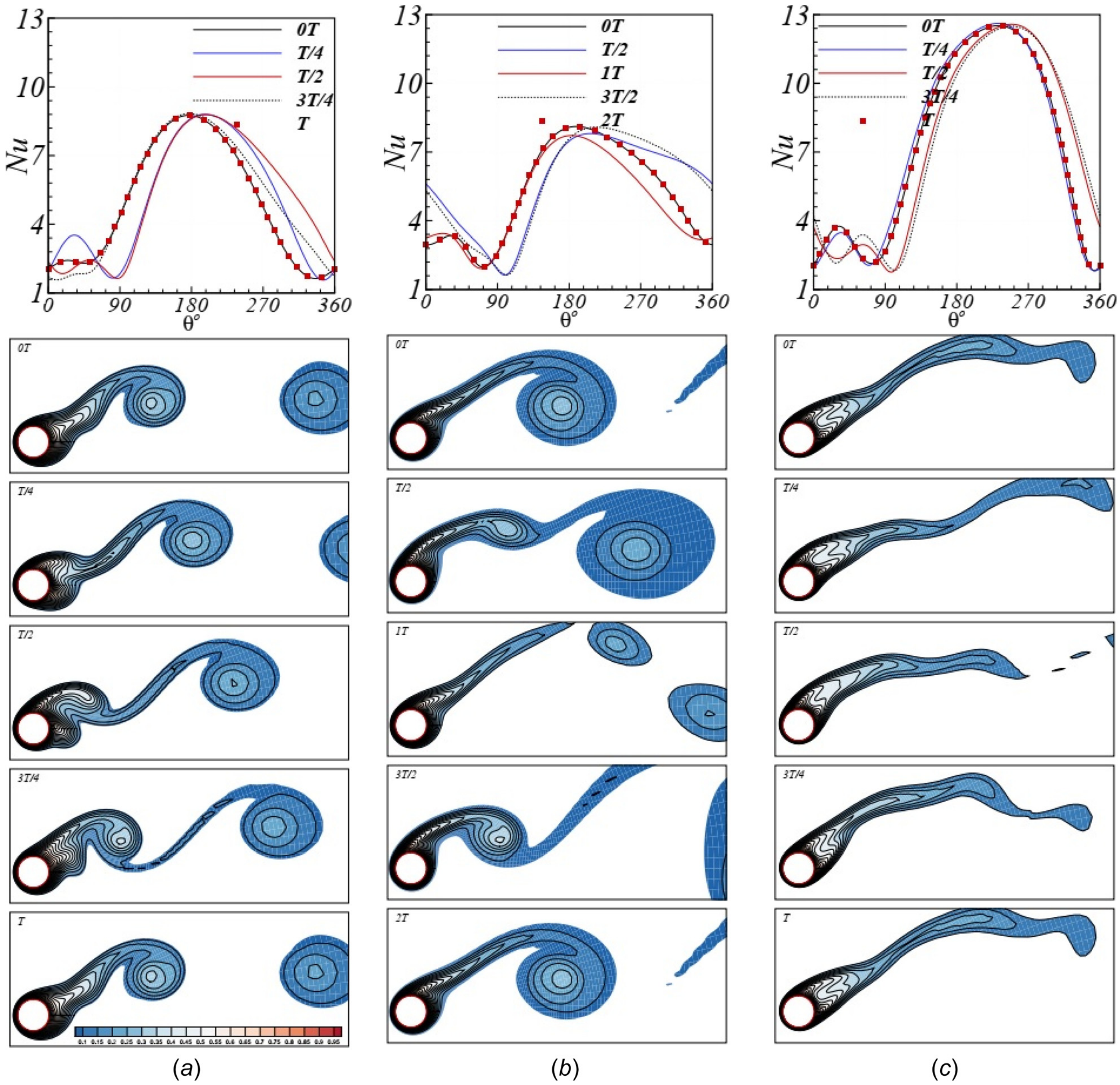

Fig. 8 The variation of local Nusselt number, *Nu*, along surface of the cylinder and the isotherm contours over: (*a*) one period of cylinder oscillation, *T*, for $K = 0.05$, (*b*) two periods of oscillation, 2 *T* for $K = 0.1$, and (*c*) one period of oscillation, *T*, for $K = 0.15$; at $Re = 100$, $\alpha_m = 1.0$ and $f_r = 1.0$

this maximum peak shifts to $\theta \approx 204\,\mathrm{deg}$ as compare to $\theta \approx 180\,\mathrm{deg}$ (corresponding to $K = 0.05$). The distribution of the Nusselt number curve at the lower half surface of the cylinder ($180\,\mathrm{deg} < \theta <$ deg) is significantly different from the distribution of the Nusselt number curve at the upper half ($0\,\mathrm{deg} < \theta < 180\,\mathrm{deg}$). It is observed that the lower half generates more heat than the upper half which can be attributed to relatively lesser fluid velocity near the lower half than the upper half. Therefore shear rate can significantly alter the dynamics of the heat transfer mechanism.

Further increase in K to 0.15 in Fig. 7 leads to a full vortex shedding suppression. The isotherm contours are elongated in the stream-wise direction showing nil development of vortex. Vortex shedding suppression is also been observed for the case of rotating cylinder by [21–24,49,58,59]. The value of maximum peaks in the Nusselt number distribution plot is observed to oscillate in the range $180\,\mathrm{deg} < \theta < 270\,\mathrm{deg}$. The value of this maximum peak is the highest amongst $K = 0.05$ and $K = 0.1$ cases. The distribution of Nu curves in the lower half is different from that in the upper half, similar to the case when $K = 0.1$. However, the elongation of the wake causes some increment in the heat transfer at the surface of the cylinder in $40\,\mathrm{deg} < \theta < 70\,\mathrm{deg}$, which is apparent from the additional local maximum peak there. No such vortex shedding suppression is observed for the case of nonshear flow (Ref. [20]) corresponding to the same set of numerical parameter values.

In Fig. 8, when the oscillation amplitude, α_m, increases to 1.0, the vortex shedding modes are identified as $1S(T)$, $2S(2T)$ corresponding to $K = 0.05$, 0.1 , respectively. In this case also, the size of the vortices increases with an increase in K value up to 0.1. Interestingly, it is observed from the isotherm contours corresponding to $K = 0.05$ that the vortex that begins to develop from the lower surface of the cylinder eventually merges into the wake without getting detached. The development of vortices from the lower surface ($180\,\mathrm{deg} < \theta < 360\,\mathrm{deg}$) of the cylinder tend to cease with increasing K till $K = 0.1$ leading to nil generation of vortices from both sides when $K = 0.15$. Similar partial vortex shedding suppression is observed by Chew et al. [49] for the case

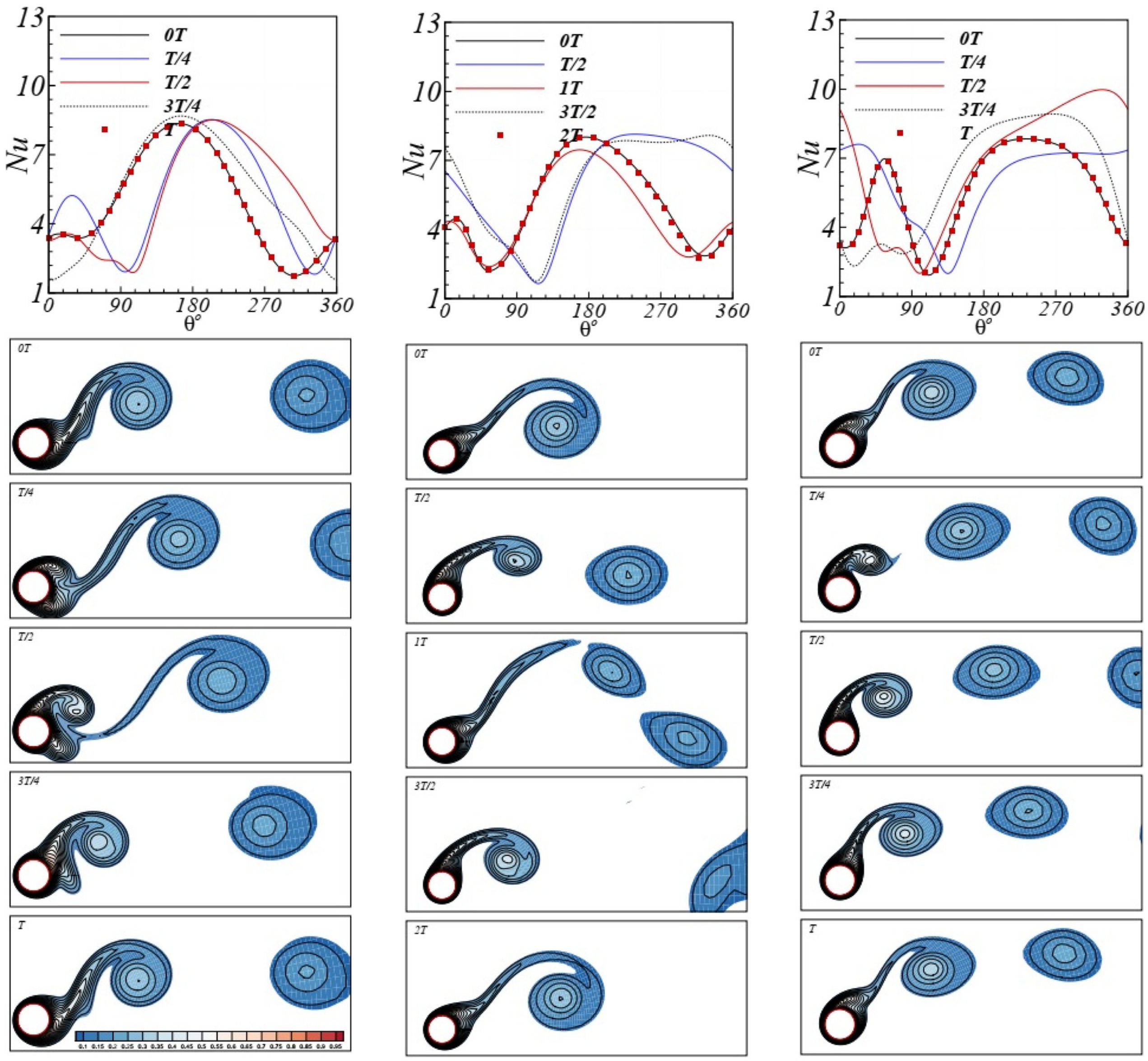

Fig. 9 The variation of local Nusselt number, Nu, along surface of the cylinder and the isotherm contours over: (*a*) one period of cylinder oscillation, T, for $K = 0.05$, (*b*) two periods of oscillation, $2\,T$ for $K = 0.1$, and (*c*) one period of oscillation, T, for $K = 0.15$; at $Re = 100$, $\alpha_m = 2.0$ and $f_r = 1.0$

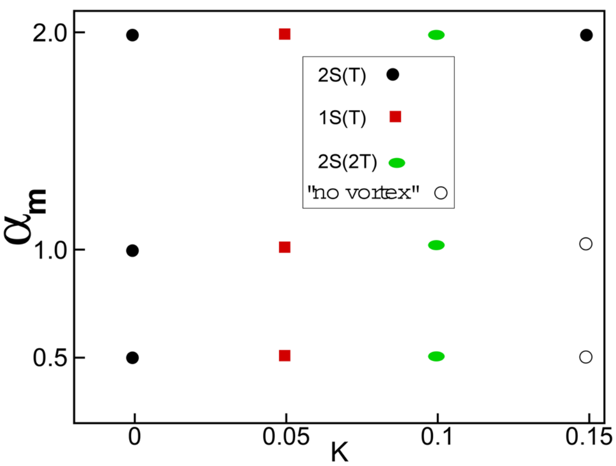

Fig. 10 A summary of the locked-on vortex shedding modes for $f_r = 1.0$, $K\in[0.0, 0.15]$ and $\alpha_m\in[0.5, 2.0]$ for $Re = 100$

of rotating circular cylinder. The phenomenon of heat transfer has a similar description to that obtained at $\alpha_m = 0.5$. However, the value of the maximum peak in the Nusselt number distribution plot increases for $\alpha_m = 1.0$ relative to $\alpha_m = 0.5$ case, corresponding to all considered K values.

With further increase in α_m to 2.0 (Fig. 9), the vortex shedding modes are identified as $1S(T), 2S(2T), 2S(T)$ corresponding to $K = 0.05, 0.1, 0.15$, respectively. A first inspection of the isotherm contours reveals that vortices are shed only from the upper surface of the cylinder, for all K values. It is observed that the size of the vortices decreases with increasing K continuously as opposite to the previous values of α_m, where the size first increases up to $K = 0.1$ and then decreases. As K increases, the vortex development length in the stream-wise direction shortens where more number of vortices are seen in the wake. This is due to the combined effect of large K value and high rotation rates leading to complex flow structure. Similar shortening of the vortex development length is observed by Mittal and Al-Mdallal [20] for nonshear flow case with increasing the frequency ratio f_r. The values of maximum peaks in Nu plots for $\alpha_m = 2.0$ are minimum amongst $\alpha_m = 0.5$ and 1.0 cases corresponding to all considered K values. Significant fluctuations in the maximum-minimum peaks in Nu plots are seen during the cylinder oscillation period at a high shear rate $K = 0.15$. The locations and values of the maximum peaks show a substantial change during the cylinder oscillation period for $K = 0.15$. Maximum peak is observed at $\theta \approx 324\,\deg$ when the cylinder completes half of its oscillation period. This observation is attributed to both the high shear rate and large oscillation amplitude of the cylinder oscillation which will definitely affect the structure of the fluid attached to the cylinder.

Figure 10 summarizes the locked-on vortex shedding modes for $f_r = 1.0$, $K \in [0.0, 0.15]$ and $\alpha_m \in [0.5, 2.0]$ at $Re = 100$. When the inflow freestream is a shear flow, the vortex shedding from the surface of the cylinder over one period of cylinder oscillation gets delayed relative to the nonshear case. For instance, two vortices are shed from the surface of the cylinder over one oscillation period for nonshear case ($K = 0.0$) while one vortex is shed during one oscillation period for shear flow. The number of vortices that are being shed during one oscillation period does not change with α_m for the fixed value of K. Full vortex shedding suppression is observed for $K = 0.15$ and $\alpha_m < 2.0$. The vortex shedding mode for $K = 0.15, \alpha_m = 2.0$ is similar to the nonshear case $(0.5 \leq \alpha_m \leq 2.0)$.

Figure 11(*a*) shows the effect of K on the variation of local Nusselt number over cylinder surface for $\alpha_m = 0.5, f_r = 1.0$ at $Re = 100$. For nonshear flow, the variation of local Nusselt number shows the maximum peak at $\theta \approx 180^\circ$. For shear flow, the value of the maximum peak decreases with increasing K up to $K \leq 0.1$ and increases again for $K = 0.15$, where it attains the maximum value. The location of the maximum peak for $K = 0.0, 0.05$ and 0.1 is nearly the same but a significant shift in the location of the maximum peak along the cylinder surface is observed for $K = 0.15$. Similar observations are documented by Yan and Zu [60] for the cylinder rotating in a nonshear flow and by Nemati et al. [53] for the cylinder rotating in a shear flow. The effect of rotational parameter α_m on the average heat transfer rate can be observed from Fig. 11(*b*) for different values of K. α_m plays a significant role in the heat transfer phenomenon for the higher shear rate $K = 0.15$. When $K = 0.15$, heat transfer rate increases significantly from 6.5071 ($\alpha_m = 0.5$) to 7.3052 ($\alpha_m = 1.0$) followed by a sudden drop to 5.5650 ($\alpha_m = 2.0$). Extraordinary fluctuating behavior is attributed to a very high shear rate and the oscillation of the cylinder surface. This may be due to the fact that the background vorticity in the freestream dominates the vorticity generated from the cylinder surface which is unlikely for the low shear rate.

In order to describe the effect of Prandtl number, Pr, on heat transfer, the variation of local Nusselt number on the surface of cylinder for different values of Pr and $\alpha_m = 2.0, f_r = 1.0$ at $K = 0.1$ in Fig. 12(*a*). With increase in Pr, Nu plot shows a translation toward positive $y-$axis, similar to the nonshear flow case (Refs. [20,24]) and the locations of maximum peaks are also the same. The effect of Pr on the overall heat transfer can be seen from Fig. 12(*b*) for both shear and nonshear flows. The time-averaged values of heat transfer rate for $\alpha_m = 1.0, f_r = 1.0$, and

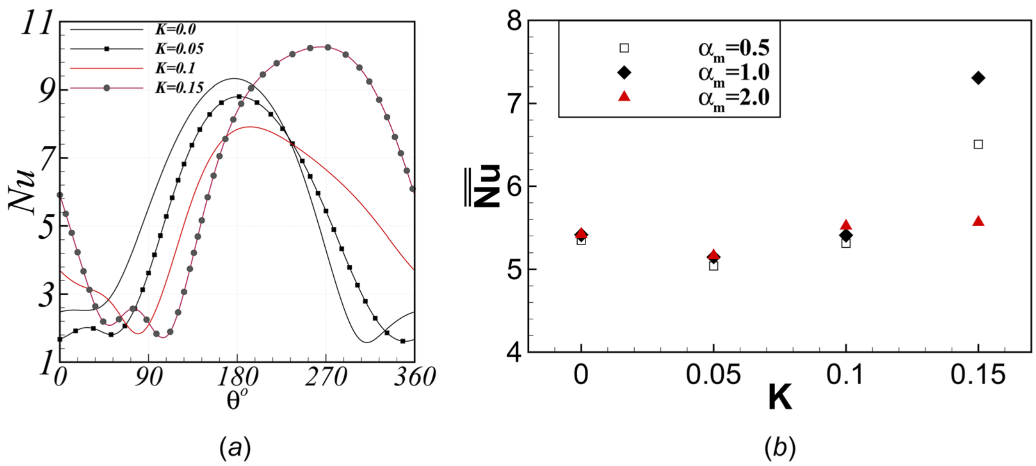

Fig. 11 The variation of: (*a*) the local Nusselt number, *Nu*, along surface of the cylinder for different *K* values at $\alpha_m = 0.5$ and (*b*) the time average Nusselt number versus shear rate, *K*, of oscillating cylinder at different values of α_m for $Re = 100$, $f_r = 1.0$

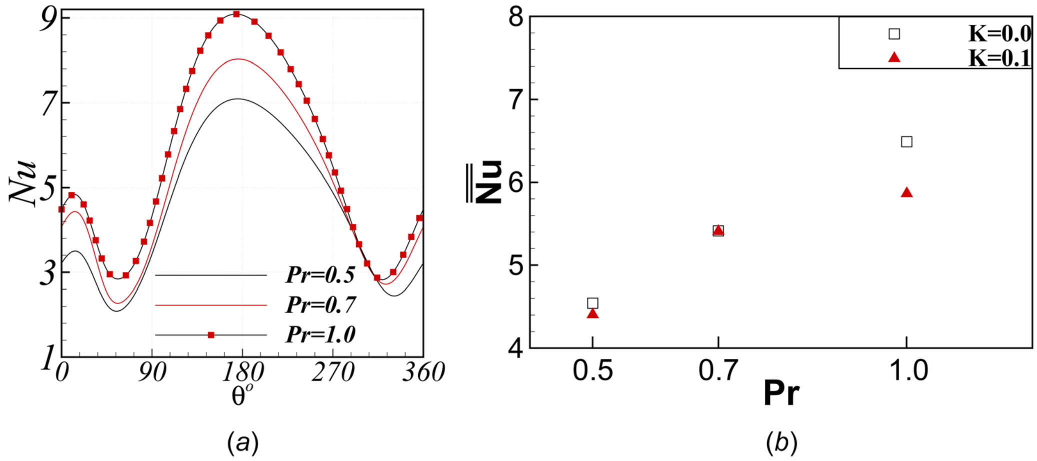

Fig. 12 Effect of Pr on: (a) the variation of local Nusselt number at time period $t=2T$ for $K=0.1, \alpha_m=2.0$ and (b) the variation of time average Nusselt number for $K=0.0, 0.1, \alpha_m=1.0$ for $Re=100, f_r=1.0$

$K=0.1$ are 4.4052, 5.4085, and 5.8653 for $Pr=0.5, 0.7$ and 1.0, respectively. The values increase by 22.77% when Pr increases from 0.5 to 0.7 and 8.45% when Pr increases from 0.7 to 1.0. However, for the nonshear flow case the change are 19.17% when Pr increases from 0.5 to 0.7, 19.84% when Pr increases from 0.7 to 1.0.

6 Conclusion

This study numerically investigates the heat transfer from a two-dimensional isothermal circular cylinder rotational oscillations in a linear shear flow. The coupled governing equations of flow and heat transfer are solved by using higher order compact finite difference scheme. The simulations are performed for $Re=100, Pr=0.5-1.0, \alpha_m \in [0.5, 2.0], f_r=1.0,$ and $K \in [0.0, 0.15]$ to address an increase or decrease in the heat transfer rate relative to nonshear flow. The introduction of shear at the inlet causes a troublesome interaction of the free shear layer with the boundary layer of the cylinder due to background vorticity in the freestream. This phenomenon alters the wake structure, vortex shedding and heat transfer mechanism in a significant way. The numerical results reveal that shearing of the inlet freestream can lead to partial or full vortex shedding suppression from the surface of the cylinder for a fixed rotational speed. New findings are uncovered at high shear rates where a pronounced increase in the heat transfer rate is reported at certain values of rotational speed ($\alpha_m=0.5, 1.0$), relative to the nonshear flow. A reduction in the heat transfer rate is reported at a low shear rate ($K=0.05$) for all considered values of α_m, relative to the nonshear flow case. However, the heat transfer rate increases with an increase in the values of K ($K>0$) for all considered values of α_m. For high shear rate ($K=0.15$), a significant increase in the heat transfer rate is observed when α_m increases ($0.5 \le \alpha_m \le 1.0$) followed by a sudden drop to minimum ($1.0 \le \alpha_m \le 2.0$).

Future work encompasses a comprehensive study of the heat transfer mechanisms for a wide range of frequency ratios (f_r), Reynolds numbers (Re) to draw more general conclusions.

Funding Data

- University Grants Commission (Grant No. No.F.4-2/2006 (BSR)/MA/18-19/0095; Funder ID: 10.13039/501100001501).

Nomenclature

$f =$ dimensionless oscillation frequency ($= R_0\tilde{f}/U_\infty$)
$f_0 =$ natural frequency of vortex shedding i.e. vortex shedding frequency for fixed circular cylinder($\alpha_m=0$) in nonshear flow ($K=0$)
$f_r =$ frequency ratio ($= f/f_0$)
$\tilde{f} =$ dimensional oscillation frequency
$h, \overline{h} =$ local and average heat transfer coefficient
$K =$ shear rate
$k =$ thermal conductivity
$Nu, \overline{Nu} =$ local and average Nusselt number
$\overline{\overline{Nu}} =$ time averaged Nusselt number
$Pr =$ Prandtl number
$R_0 =$ radius of the circular cylinder
$R_\infty =$ radius of the circular far-field boundary
$Re =$ Reynolds number ($= 2R_0U_\infty/\nu$)
$r, \theta =$ Polar coordinates
$t =$ dimensionless time ($= \tau U_\infty/R_0$)
$T =$ oscillation period of the cylinder
$T_s =$ temperature of the surface of the cylinder
$u =$ dimensionless radial velocity
$U_o =$ space-averaged centerline velocity at inlet
$U_\infty =$ free stream velocity
$v =$ dimensionless tangential velocity
$x, y =$ Cartesian coordinates
$\alpha =$ dimensionless oscillatory velocity ($= R_0\tilde{\alpha}/U_\infty$)
$\tilde{\alpha} =$ dimensional oscillatory velocity
$\tilde{\alpha}_m =$ dimensional oscillation amplitude
$\alpha_m =$ dimensionless oscillation amplitude ($= R_0\tilde{\alpha}_m/U_\infty$)
$\Delta t =$ time step
$\nu =$ kinematic viscosity of the fluid
$\psi =$ dimensionless stream function
$\omega =$ dimensionless vorticity

Appendix 1

$$C11_{ij} = H_{12}Re - 0.5\Delta tA1_{ij}, C21_{ij} = H_{12}Re + 0.5\Delta tC1_{ij},$$
$$C12_{ij} = r_i^2K_{12}Re - 0.5\Delta tA2_{ij}, C22_{ij} = r_i^2K_{12}Re + 0.5\Delta tC2_{ij},$$
$$C13_{ij} = Re(H_{11} - c_1H_{12}) - 0.5\Delta tC3_{ij},$$
$$C23_{ij} = Re(H_{11} - c_1H_{12}) + 0.5\Delta tC3_{ij},$$
$$C14_{ij} = r_i^2Re(K11 + r_iRev_{i,j}K_{12}) - 0.5\Delta tC4_{ij},$$
$$C24_{ij} = r_i^2Re(K11 + r_iRev_{i,j}K_{12}) + 0.5\Delta tC4_{ij},$$
$$C15_{ij} = -0.5\Delta tC5_{ij}, C25_{ij} = 0.5\Delta tC5_{ij},$$
$$C16_{ij} = -0.5\Delta tC6_{ij}, C26_{ij} = 0.5\Delta tC6_{ij},$$
$$C17_{ij} = -0.5\Delta tC7_{ij}, C27_{ij} = 0.5\Delta tC7_{ij},$$
$$C18_{ij} = -0.5\Delta tC8_{ij}, C28_{ij} = 0.5\Delta tC8_{ij},$$

where,

$$C1_{ij} = 1 - 0.5c_1(r_f - r_b) - (H_{12}c_1^2 - c_1H_{11}) - 2H_{12}\left(Re(u_r)_{ij} + \frac{1}{r_i^2}\right),$$

$$C2_{ij} = \frac{1}{r_i^2} + 0.5d_1(\theta_f - \theta_b) - \frac{2}{r_i^3}(H_{11} - H_{12}c_1) + \frac{6H_{12}}{r_i^4} - Rev_{ij}r_i(K_{11} + Rev_{ij}r_iK_{12}) - 2K_{12}Re(v_\theta)_{ij}r_i,$$

$$C3_{ij} = c_1 - (H_{11} - c_1H_{12})\left(Re(u_r)_{ij} + \frac{1}{r_i^2}\right) - H_{12}\left(Re(u_{rr})_{ij} - \frac{2}{r_i^3}\right) - Re(u_\theta)_{ij}r_i^2(K_{11} + Rev_{ij}r_iK_{12}) - K_{12}Re(v_{\theta\theta})_{ij}r_i^2,$$

$$C4_{ij} = -d_1 - (H_{11} - c_1H_{12})\left((v_r)_{ij}r_i - v_{ij}\right)\frac{Re}{r_i^3} - H_{12}\left((v_{rr})_{ij}r_i^2 - 2(v_r)_{ij}r_i + 2v_{ij}\right)\frac{Re}{r_i^3} - Re(v_\theta)_{ij}r_i(K_{11} + Rev_{ij}r_iK_{12}) - K_{12}Re(v_\theta\theta)_{ij}r_i,$$

$$C5_{ij} = -d_1(H_{11} - c_1H_{12}) - 2H_{12}\left((v_r)_{ij}r_i - v_{ij}\right)\frac{Re}{r_i^2} + c_1r_i^2(K_{11} + Rev_{ij}r_iK_{12}) - 2K_{12}Re(v_\theta)_{ij}r_i^2,$$

$$C6_{ij} = (H_{11} - c_1H_{12})\frac{1}{r_i^2} - \frac{4H_{12}}{r_i^3} + c_1K_{12}r_i^2,$$

$$C7_{ij} = -d_1H_{12} + r_i^2(K_{11} + Rev_{ij}r_iK_{12}),$$

$$C8_{ij} = \frac{H_{12}}{r_i^2} + K_{12}r_i^2,$$

$$H_{11} = \frac{1}{6}\left\{2(r_f - r_b) + cr_fr_b\right\},$$

$$H_{12} = \frac{1}{24}\left\{2(r_f^2 + r_b^2 - r_fr_b) + cr_fr_b(r_f - r_b)\right\},$$

$$K_{11} = \frac{1}{6}\left\{\frac{2}{r_i^2}(\theta_f - \theta_b) - d\theta_f\theta_b\right\}$$

Appendix 2

The expressions for the finite difference operators appearing in the above equations are as follows:

$$\delta_r\phi_{i,j} = \frac{\phi_{i+1,j} - \phi_{i-1,j}}{2\Delta r},$$

$$\delta_\theta\phi_{i,j} = \frac{\phi_{i,j+1} - \phi_{i,j-1}}{2\Delta\theta},$$

$$\delta_r^2\phi_{i,j} = \frac{1}{\Delta r}\left\{\frac{\phi_{i+1,j}}{r_f} - \left(\frac{1}{r_f} + \frac{1}{r_b}\right)\phi_{i,j} + \frac{\phi_{i-1,j}}{r_b}\right\},$$

$$\delta_\theta^2\phi_{i,j} = \frac{1}{\Delta\theta}\left\{\frac{\phi_{i,j+1}}{\theta_f} - \left(\frac{1}{\theta_f} + \frac{1}{\theta_b}\right)\phi_{i,j} + \frac{\phi_{i,j-1}}{\theta_b}\right\},$$

$$\delta_r^2\delta_\theta\phi_{i,j} = \frac{1}{2\Delta r\Delta\theta}\left\{\frac{1}{r_f}(\phi_{i+1,j+1} - \phi_{i+1,j-1}) - \left(\frac{1}{r_f} + \frac{1}{r_b}\right)(\phi_{i,j+1} - \phi_{i,j-1}) + \frac{1}{r_b}(\phi_{i-1,j+1} - \phi_{i-1,j-1})\right\},$$

$$\delta_r\delta_\theta^2\phi_{i,j} = \frac{1}{2\Delta r\Delta\theta}\left\{\frac{1}{\theta_f}(\phi_{i+1,j+1} - \phi_{i-1,j+1}) - \left(\frac{1}{\theta_f} + \frac{1}{\theta_b}\right)(\phi_{i+1,j} - \phi_{i-1,j}) + \frac{1}{\theta_b}(\phi_{i+1,j-1} - \phi_{i-1,j-1})\right\},$$

$$\delta_r^2\delta_\theta^2\phi_{i,j} = \frac{1}{\Delta r\Delta\theta}\left\{\frac{\phi_{i+1,j+1}}{r_f\theta_f} + \frac{\phi_{i-1,j+1}}{r_b\theta_f} - \left(\frac{1}{r_f\theta_f} + \frac{1}{r_b\theta_f}\right)\phi_{i,j+1} - \left(\frac{1}{r_f\theta_f} + \frac{1}{r_f\theta_b}\right)\phi_{i+1,j}\right.$$
$$\left. + \left(\frac{1}{r_f\theta_f} + \frac{1}{r_f\theta_b} + \frac{1}{r_b\theta_f} + \frac{1}{r_b\theta_b}\right)\phi_{i,j} - \left(\frac{1}{r_f\theta_b} + \frac{1}{r_b\theta_b}\right)\phi_{i,j-1} - \left(\frac{1}{r_b\theta_f} + \frac{1}{r_b\theta_b}\right)\phi_{i-1,j} + \frac{\phi_{i+1,j-1}}{r_f\theta_b} + \frac{\phi_{i-1,j-1}}{r_b\theta_b}\right\}, \delta_r\delta_\theta\phi_{i,j}$$
$$= \frac{1}{4\Delta r\Delta\theta}\left\{\phi_{i+1,j+1} - \phi_{i+1,j-1} - \phi_{i-1,j+1} + \phi_{i-1,j-1}\right\},$$

where, $r_f = (r_{i+1} - r_i), r_b = (r_i - r_{i-1}), \theta_f = (\theta_{j+1} - \theta_j), \theta_b = (\theta_j - \theta_{j-1}), \Delta r = \frac{r_f + r_b}{2}$ and $\Delta\theta = \frac{\theta_f + \theta_b}{2}$.

References

[1] Kalita, J. C., and Ray, R. K., 2009, "A Transformation-Free Hoc Scheme for Incompressible Viscous Flows Past an Impulsively Started Circular Cylinder," J. Comput. Phy., **228**(14), pp. 5207–5236.

[2] Mittal, H., 2016, "A Class of Higher Order Accurate Schemes for Fluid Interface Problems," Ph.D. thesis, Indian Institute of Technology, Mandi, India.

[3] Ray, R. K., and Kalita, J. C., 2016, "Higher-Order-Compact Simulation of Unsteady Flow Past a Rotating Cylinder at Moderate Reynolds Numbers," Comput. Appl. Math., **35**(1), pp. 219–250.

[4] Mittal, H., Ray, R. K., and Al-Mdallal, Q. M., 2017, "A Numerical Study of Initial Flow Past an Impulsively Started Rotationally Oscillating Circular Cylinder Using a Transformation-Free Hoc Scheme," Phys. Fluids, **29**(9), p. 093603.

[5] Mittal, H., Al-Mdallal, Q. M., and Ray, R. K., 2017, "Locked-on Vortex Shedding Modes From a Rotationally Oscillating Circular Cylinder," Ocean Eng., **146**, pp. 324–338.

[6] Kumar, A., 2019, "Unsteady Flow Separation from the Surface of Solid Cylinders in Laminar Shear Flow: A Structural Bifurcation Analysis," Ph.D. thesis, IIT Mandi, Mandi, India.

[7] Kumar, A., and Ray, R. K., 2019, "Structural Bifurcation Analysis of Vortex Shedding From Shear Flow Past Circular Cylinder," Comput. Appl. Math., **38**(3), p. 121.

[8] Sellappan, P., and Pottebaum, T., 2014, "Vortex Shedding and Heat Transfer in Rotationally Oscillating Cylinders," J. Fluid Mech., **748**, pp. 549–579.

[9] Strouhal, V., 1878, "Über Eine Besondere Art Der Tonerregung," Annalen Der Phys., **241**(10), pp. 216–251.

[10] Kumar, S., Lopez, C., Probst, O., Francisco, G., Askari, D., and Yang, Y., 2013, "Flow Past a Rotationally Oscillating Cylinder," J. Fluid Mech., **735**, pp. 307–346.

[11] Lu, X.-Y., and Sato, J., 1996, "A Numerical Study of Flow Past a Rotationally Oscillating Circular Cylinder," J. Fluids Struct., **10**(8), pp. 829–849.

[12] Gao, Y-y., Yin, C-s., Yang, K., Zhao, X-Z., and Tan, S. K., 2017, "Experimental Study on Flow Past a Rotationally Oscillating Cylinder," China Ocean Eng., **31**(4), pp. 495–503.

[13] Yawar, A., Ebrahem, M., Manzoor, S., Sheikh, N., and Ali, M., 2019, "Transient Cross Flow and Heat Transfer Over a Rotationally Oscillating Cylinder Subjected to Gust Impulse," Int. J. Heat Mass Transfer, **137**, pp. 108–123.

[14] Ganta, N., Mahato, B., and Bhumkar, Y. G., 2019, "Analysis of Sound Generation by Flow Past a Circular Cylinder Performing Rotary Oscillations Using Direct Simulation Approach," Phys. Fluids, **31**(2), p. 026104.

[15] Zebib, A., and Wo, Y., 1989, "A Two-Dimensional Conjugate Heat Transfer Model for Forced Air Cooling of an Electronic Device," ASME. J. Electron. Packag., **111**(1), pp. 41–45.

[16] Yang, R.-J., and Fu, L.-M., 2001, "Thermal and Flow Analysis of a Heated Electronic Component," Int. J. Heat Mass Transfer, **44**(12), pp. 2261–2275.

[17] Ganesan, P., and Loganathan, P., 2001, "Unsteady Natural Convective Flow Past a Moving Vertical Cylinder With Heat and Mass Transfer," Heat Mass Transfer, **37**(1), pp. 59–65.

[18] Takhar, H. S., Chamkha, A. J., and Nath, G., 2000, "Combined Heat and Mass Transfer Along a Vertical Moving Cylinder With a Free Stream," Heat Mass Transfer, **36**(3), pp. 237–246.

[19] Mahfouz, F., and Badr, H., 2000, "Forced Convection From a Rotationally Oscillating Cylinder Placed in a Uniform Stream," Int. J. Heat Mass Transfer, **43**(17), pp. 3093–3104.

[20] Mittal, H., and Al-Mdallal, Q. M., 2018, "A Numerical Study of Forced Convection From an Isothermal Cylinder Performing Rotational Oscillations in a Uniform Stream," Int. J. Heat Mass Transfer, **127**, pp. 357–374.

[21] Bouakkaz, R., Talbi, K., Ouazzazi, M., Khelili, Y., and Salhi, F., 2015, "Effect of Rotation Rates on the Laminar Flow and Heat Transfer Past a Circular Cylinder," Braz. J. Chem. Eng., **32**(2), pp. 519–529.

[22] Paramane, S. B., and Sharma, A., 2009, "Numerical Investigation of Heat and Fluid Flow Across a Rotating Circular Cylinder Maintained at Constant Temperature in 2-d Laminar Flow Regime," Int. J. Heat Mass Transfer, **52**(13–14), pp. 3205–3216.

[23] Ghazanfarian, J., and Nobari, M., 2009, "A Numerical Study of Convective Heat Transfer From a Rotating Cylinder With Cross-Flow Oscillation," Int. J. Heat Mass Transfer, **52**(23–24), pp. 5402–5411.

[24] Nobari, M., and Ghazanfarian, J., 2010, "Convective Heat Transfer From a Rotating Cylinder With Inline Oscillation," Int. J. Therm. Sci., **49**(10), pp. 2026–2036.

[25] Singh, S., and Mittal, S., 2005, "Flow Past a Cylinder: Shear Layer Instability and Drag Crisis," Int. J. Numer. Methods Fluids, **47**(1), pp. 75–98.

[26] Saxena, U., and Laird, A., 1978, "Heat Transfer From a Cylinder Oscillating in a Cross-Flow," ASME J. Heat Transfer-Trans. ASME, **100**(4), pp. 684–689.

[27] Leung, C., Ko, N., and Ma, K., 1981, "Heat Transfer From a Vibrating Cylinder," J. Sound Vib., **75**(4), pp. 581–582.

[28] Childs, E., and Mayle, R., 1984, "Heat Transfer on a Rotationally Oscillating Cylinder in Crossflow," Int. J. Heat Mass Transfer, **27**(1), pp. 85–94.

[29] Cheng, C.-H., Chen, H.-N., and Aung, W., 1997, "Experimental Study of the Effect of Transverse Oscillation on Convection Heat Transfer From a Circular Cylinder," ASME J. Heat Transfer-Trans. ASME, **119**(3), pp. 474–482.

[30] Fu, W.-S., and Tong, B.-H., 2002, "Numerical Investigation of Heat Transfer From a Heated Oscillating Cylinder in a Cross Flow," Int. J. Heat Mass Transfer, **45**(14), pp. 3033–3043.

[31] Beskok, A., Raisee, M., Celik, B., Yagiz, B., and Cheraghi, M., 2012, "Heat Transfer Enhancement in a Straight Channel Via a Rotationally Oscillating Adiabatic Cylinder," Int. J. Therm. Sci., **58**, pp. 61–69.

[32] Al-Mdallal, Q., and Mahfouz, F., 2017, "Heat Transfer From a Heated Non-Rotating Cylinder Performing Circular Motion in a Uniform Stream," Int. J. Heat Mass Transfer, **112**, pp. 147–157.

[33] Jordan, S. K., and Fromm, J. E., 1972, "Laminar Flow Past a Circle in a Shear Flow," Phys. Fluids, **15**(6), pp. 972–976.

[34] Cao, S., Hirano, K., Ozono, S., and Wakasugi, Y., 2000, "Vortex Shedding for a Circular Cylinder Placed in Strong Shear Flow," J. Wind Eng., **25**(4), pp. 85_53–62.

[35] Cao, S., and Tamura, Y., 2008, "Flow Around a Circular Cylinder in Linear Shear Flows at Subcritical Reynolds Number," J. Wind Eng. Indus. Aerodyn., **96**(10–11), pp. 1961–1973.

[36] Cao, S., Ozono, S., Tamura, Y., Ge, Y., and Kikugawa, H., 2010, "Numerical Simulation of Reynolds Number Effects on Velocity Shear Flow Around a Circular Cylinder," J. Fluids Struct., **26**(5), pp. 685–702.

[37] Wu, T., and Chen, C.-F., 2000, "Laminar Boundary-Layer Separation Over a Circular Cylinder in Uniform Shear Flow," Acta Mech., **144**(1–2), pp. 71–82.

[38] Lei, C., Cheng, L., and Kavanagh, K., 2000, "A Finite Difference Solution of the Shear Flow Over a Circular Cylinder," Ocean Eng., **27**(3), pp. 271–290.

[39] Sumner, D., and Akosile, O., 2003, "On Uniform Planar Shear Flow Around a Circular Cylinder at Subcritical Reynolds Number," J. Fluids Struct., **18**(3–4), pp. 441–454.

[40] Kappler, M., Rodi, W., Szepessy, S., and Badran, O., 2005, "Experiments on the Flow Past Long Circular Cylinders in a Shear Flow," Exp. Fluids, **38**(3), pp. 269–284.

[41] Kim, D., Choi, H., and Choi, H., 2005, "Characteristics of Laminar Flow Past a Sphere in Uniform Shear," Phys. Fluids, **17**(10), p. 103602.

[42] Kang, S., 2006, "Uniform-Shear Flow Over a Circular Cylinder at Low Reynolds Numbers," J. Fluids Struct., **22**(4), pp. 541–555.

[43] Omori, T., Jakirlić, S., Tropea, C., and Obi, S., 2008, "Shearless and Sheared Flow Past a circular cylinder: Comparative Analysis by Means of Les," Int. J. Heat Fluid Flow, **29**(3), pp. 703–720.

[44] Zhang, H., Fan, B-c., Chen, Z-h., Li, H-Z., and Li, B-m., 2014, "An in-Depth Study on Vortex-Induced Vibration of a Circular Cylinder With Shear Flow," Comput. Fluids, **100**, pp. 30–44.

[45] Yoshino, F., and Hayashi, T., 1984, "The Numerical Solution of Flow Around a Rotating Circular Cylinder in Uniform Shear Flow," Bull. JSME, **27**(231), pp. 1850–1857.

[46] Kurose, R., and Komori, S., 1999, "Drag and Lift Forces on a Rotating Sphere in a Linear Shear Flow," J. Fluid Mech., **384**(1), pp. 183–206.

[47] Kang, S., 2006, "Laminar Flow Over a Steadily Rotating Circular Cylinder Under the Influence of Uniform Shear," Phys. Fluids, **18**(4), p. 047106.

[48] Rohlf, K., and D'Alessio, S., 2005, "Uniform Shear Flow Past a Circular Cylinder," Acta Mech., **178**(3–4), pp. 199–222.

[49] Chew, Y., Luo, S., and Cheng, M., 1997, "Numerical Study of a Linear Shear Flow Past a Rotating Cylinder," J. Wind Eng. Indus. Aerodyn., **66**(2), pp. 107–125.

[50] Stansby, P., 1976, "The Locking-on of Vortex Shedding Due to the Cross-Stream Vibration of Circular Cylinders in Uniform and Shear Flows," J. Fluid Mech., **74**(4), pp. 641–665.

[51] Shi, J.-M., Breuer, M., and Durst, F., 2002, "Wall Effect on Heat Transfer From a Micro-Cylinder in Near-Wall Shear Flow," Int. J. Heat Mass Transfer, **45**(6), pp. 1309–1320.

[52] Abdella, K., and Nalitolela, P., 2008, "Approximate Analytic Solutions for Forced Convection Heat Transfer From a Shear-Flow Past a Rotating Cylinder," Appl. Math. Sci., **2**(11), pp. 497–527.

[53] Nemati, H., Farhadi, M., Sedighi, K., and Fattahi, E., 2011, "Multi-Relaxation-Time Lattice Boltzman Model for Uniform-Shear Flow Over a Rotating Circular Cylinder," Therm. Sci., **15**(3), pp. 859–878.

[54] Ongoren, A., and Rockwell, D., 1988, "Flow Structure From an Oscillating Cylinder Part 1. mechanisms of Phase Shift and Recovery in the Near Wake," J. Fluid Mech., **191**(-1), pp. 197–223.

[55] Williamson, C. H., and Roshko, A., 1988, "Vortex Formation in the Wake of an Oscillating Cylinder," J. Fluids Struct., **2**(4), pp. 355–381.

[56] Al-Mdallal, Q., Lawrence, K., and Kocabiyik, S., 2007, "Forced Streamwise Oscillations of a Circular Cylinder: Locked-on Modes and Resulting Fluid Forces," J. Fluids Struct., **23**(5), pp. 681–701.

[57] Milne-Thomson, L. M., 1996, *Theoretical Hydrodynamics*, Courier Corporation, Dover Publications, INC., New York.

[58] Mittal, S., 2001, "Control of Flow Past Bluff Bodies Using Rotating Control Cylinders," J. Fluids Struct., **15**(2), pp. 291–326.

[59] Paramane, S. B., and Sharma, A., 2010, "Heat and Fluid Flow Across a Rotating Cylinder Dissipating Uniform Heat Flux in 2D Laminar Flow Regime," Int. J. Heat Mass Transfer, **53**(21–22), pp. 4672–4683.

[60] Yan, Y., and Zu, Y., 2008, "Numerical Simulation of Heat Transfer and Fluid Flow Past a Rotating Isothermal Cylinder–a Lbm Approach," Int. J. Heat Mass Transfer, **51**(9–10), pp. 2519–2536.